ACS APPLIED NANO MATERIALS
Cite This: ACS Appl. Nano Mater. 2018, 1, 3520−3530
Article
www.acsanm.org

High Breakdown Strength Polymer Nanocomposites Based on the Synergy of Nanofiller Orientation and Crystal Orientation for Insulation and Dielectric Applications

Bo Li,*,† Panagiotis I. Xidas,†,‡ and Evangelos Manias*,†

†Department of Materials Science and Engineering, The Pennsylvania State University, University Park, Pennsylvania 16802, United States

‡Department of Chemistry, Aristotle University of Thessaloniki, Thessaloniki GR 54124, Greece

Supporting Information

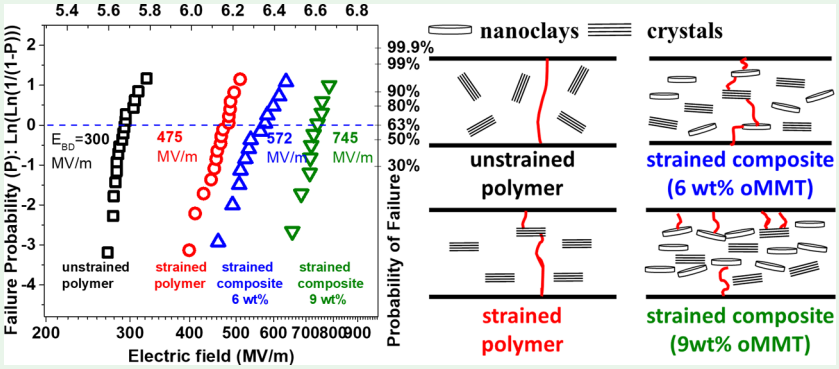

ABSTRACT: Emerging energy and insulation applications require dielectric materials that can operate at high electric fields and meanwhile possess low leakage currents. For dielectric polymer nanocomposites, beyond filler dispersion, tailoring hierarchical structures offers a promising, yet largely untapped, approach to reach this goal. Here, we demonstrate that the controlled arrangement of pseudo-2D nanofillers and polymer crystals in polyethylene/montmorillonite nanocomposites can be used as an effective approach to achieve nontrivial highly enhanced dielectric performances, far beyond what is feasible with conventional (macroscopic, isotropic) composites. In particular, it is shown that aligned nanofillers can increase the breakdown strength, while, at the same time, reducing the leakage current, in these dielectric nanostructured composites. The orientation of the nanosized pseudo-2D fillers increases the path tortuosity for charge transport, acting as an effective geometric barrier, in the same way and in addition to the oriented polymer crystals of the polymer matrix. Thus, incorporation of aligned nanoplatelet fillers provides an independent and complementary increase to breakdown strength, in excess of any improvements due to the crystal orientation. In this manner, a substantially improved breakdown strength can be realized in the nanostructured composite, with the aligned fillers and aligned polymer crystals acting as a macroscopic barrier established across the sample.

KEYWORDS: *polymer nanocomposites, dielectric breakdown, structure tailoring, crystal orientation, nanoclay orientation, montmorillonite, polyethylene*

INTRODUCTION

Dielectric materials with high breakdown strength (E_{BD}) are constantly pursued, driven by the ever-increasing requirements of miniaturization and long-term stability for electrical components in advanced electronics and electrical power systems. Many innovative approaches have been explored to improve the high field endurance of polymer dielectrics, including the construction of multilayered sandwich structures[1−4] and the cross-linking treatment for polymers.[5,6] On the other hand, introduction of inorganic insulating nanoparticles into polymers to form nanocomposite dielectrics in a controlled nanostructure[7] offers a simple and promising, yet largely untapped, approach to reach this goal. It has been reported that the addition of nanosilica,[8−10] boron nitride nanosheets,[2,11,12] or nanoclays[13,14] can increase the resistance to partial discharges and can mitigate space charge accumulation, which is responsible for the enhanced breakdown strength in these nanocomposites. The origins for such E_{BD} improvement are attributed to large interfacial areas which can trap or scatter mobile charges[15−17] and even reduce charge accumulation if the interfaces with enhanced local conductivity overlap;[18,19] the same improved high field performance can also be assigned to increased path tortuosity for e^- treeing propagation.[20,21] The latter is especially true for pseudo-2D

Received: April 24, 2018
Accepted: June 8, 2018
Published: June 8, 2018

DOI: 10.1021/acsanm.8b00671
ACS Appl. Nano Mater. 2018, 1, 3520−3530

Scheme 1. Film Production Process to Orient Nanoclays and Polymer Crystals

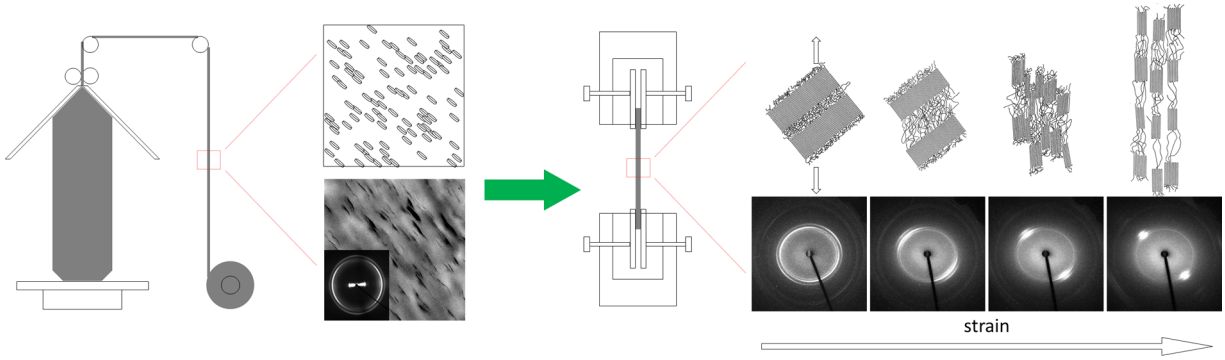

Blown Film Extrusion:
Nanoclays are aligned along the flow direction, with clay surface parallel to film surface.

Cold Stretching:
In addition to the nanoclay alignment, polymer crystals are gradually oriented along the stretching direction with increasing strain.

nanofillers with a large aspect ratio. However, most studies to date are based on isotropic composites with randomly dispersed nanofillers, and the common strategy to obtain an improved E_{BD} relies on the optimization of the composition and chemistry of fillers, filler surfactants, and polymers, leaving largely untapped opportunities for structured composites with controlled morphologies.

Recently, we have shown that the controlled alignment of montmorillonite (MMT) nanoclays perpendicular to an applied field can substantially improve the electrical properties of the structured nanocomposite compared with the respective random-filler nanocomposite and the unfilled polymer.[20] For instance, E_{BD} is enhanced from 300 MV/m for the unfilled polyethylene to 370 MV/m when the aligned nanoclays are introduced; the increase in E_{BD} is also accompanied by a dramatic improvement in reliability; i.e., low field failures are markedly eliminated in the same aligned nanocomposite. The isotropic nanocomposite with randomly dispersed fillers, while everything else remains the same as the structured counterpart, shows no improvement in E_{BD} and even a worse breakdown distribution than the polymer. The improved performance of the oriented-filler nanocomposites was shown to be related to a barrier mechanism; i.e., the orientation of the nanoclays would impose more efficient obstruction to charge carrier transport and more tortuous pathways for e^- treeing progress.[21] Following this trend, it appears that further improvement of E_{BD} should be easily achieved by increasing the concentration of aligned nanofillers, which, however, is not the case in reality. It is challenging to control the filler dispersion at high filler loadings, usually leading to less exfoliated/intercalated nanoclays (less effective barriers); besides, the microvoids trapped within filler agglomerates and the accumulation of the surfactant ions from organoclays can initiate premature failures, as observed in a recent study.[14] Polymer nanocomposites with oriented MMT nanofillers across the entire range of volume fractions—from pure polymer to pure MMT granular consolidate—are prepared by spray casting. E_{BD} of these nanocomposites increases with increasing filler concentration up to a plateau value at an intermediate filler content, followed by a decrease at high filler loadings. As a result, approaches other than manipulating filler concentrations need to be explored to further improve the breakdown strength of structured nanocomposites.

Beyond the influence of nanofillers, polymer crystallinity and crystal morphology also have significant impacts on E_{BD}. It is generally accepted that a crystalline structure consisting of extensive thick lamellae tends to show a high breakdown strength;[22−25] lamellae packed densely and oriented perpendicular to the film surface can further contribute to improving the insulation properties.[26−30] The improved breakdown strength most likely originates from the higher resistance to electrical treeing across the crystalline lamellae than through the amorphous regions, as can be revealed in TEM studies of treeing initiation.[27,31] Along these lines, biaxial orientation is still the most commonly employed approach to achieve high E_{BD} for crystalline dielectric polymer films (e.g., biaxial oriented polypropylene, BOPP). Since the improved breakdown performances in both oriented-filler nanocomposites and oriented polymers are related to a similar structural feature—densely packed morphology comprising interwoven impervious barriers—a question naturally arises whether these two contributions can be synergistically combined to provide an additive improvement in E_{BD}.

It is the focus of this paper to investigate the synergy between aligned polymer crystallites and aligned nanofillers on the breakdown strength of "structured" polymer nanocomposites. Toward this end, we systematically study the effects of the MMT nanoclay orientation and the polymer crystal orientation, separately and in combination, on the high field properties. The contributions of the aligned nanoclays and of the aligned polymer crystallites in the overall E_{BD} improvement are also quantified.

METHODS

Materials and Sample Preparation. The polyethylene (PE) used here was a Dow Integral polyolefin (a nucleated 80/20 blend of linear low-density PE/low-density PE (LLDPE/LDPE)). The nanofillers were commercially available layered-silicate organo-montmorillonites (o-MMT, Nanomer grade, purchased from Nanocor), with a nominal cation exchange capacity of 1.0 mequiv/g, organically modified by dimethyldioctadecylammonium surfactants. The organoclays were first dispersed at 25 wt % inorganic loading with a twin-screw extruder in maleic anhydride functionalized PE (a 0.26 wt % MAH-*graft*-LLDPE, $\bar{M}_w$ = 67 000 g mol^{-1} and $\bar{M}_w/\bar{M}_n$ = 6.1) to produce LLDPE masterbatches. The film production includes two steps: the film blowing process and the subsequent cold-stretching process (Scheme 1).

Nanocomposites were produced by diluting the PE-MAH/o-MMT concentrates with PE, at final 6 and 9 wt % o-MMT concentrations, on an industry blown-film line (Pliant Corporation, Chippewa Falls, WI). The temperature profile of the extruder is set at 125, 145, 175, and 175 °C from feed to nozzle. The blow-up ratios are maintained at

DOI: 10.1021/acsanm.8b00671
ACS Appl. Nano Mater. 2018, 1, 3520−3530

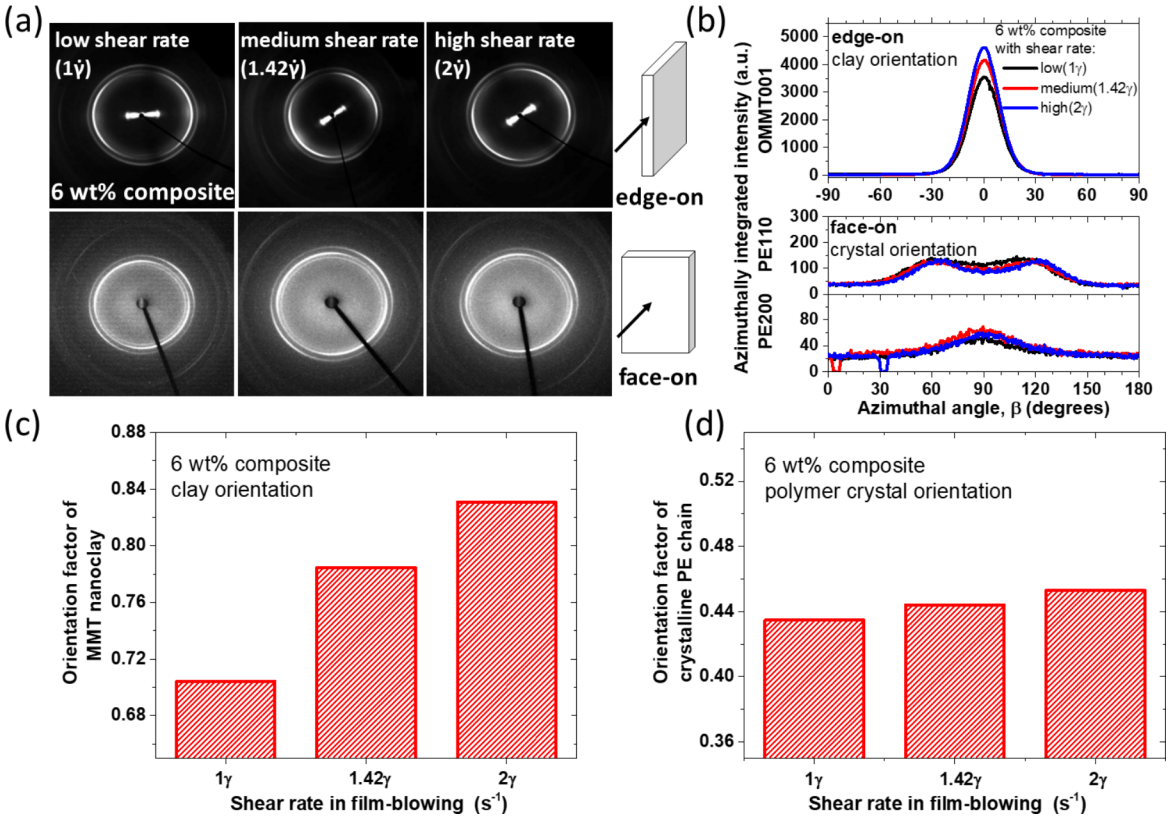

Figure 1. (a) Two-dimensional WAXD patterns for the composite films produced at different shear rates in edge-on (top) and face-on (bottom) settings. Nanofillers are highly aligned along the flow direction (azimuthal narrowing of the nanoclay diffraction patterns in the edge-on measurements (top)) and parallel to the film surface (absence of any nanoclay diffractions in the face-on measurements (bottom)). (b) Azimuthally integrated diffraction intensities from the 2D WAXD patterns shown in (a) for the nanofillers and polymer crystallites. (c) Orientation factor of the nanofillers in the composite films. Nanofiller alignment increases with increasing shear rate. (d) Orientation factor of the crystalline polymer chains in the composite films. The polymer crystals are less oriented than the nanofillers and show similar orientation in all composite films.

2 for all films, while the draw-down ratios are measured to be 6, 8, and 10 for the three 6 wt % nanocomposites and 8 for the 9 wt % nanocomposite by adjusting the take-up speed of the film. The equivalent shear rates for the 6 wt % nanocomposites are $1\dot{\gamma}$:$1.42\dot{\gamma}$:$2\dot{\gamma}$, respectively, under the processing conditions.

Films were annealed at 80 °C for 1 week and then at room temperature for another 4 weeks to relieve thermal stress and allow for full crystallization. Then the annealed films were cold-stretched along their machine direction by a tensile apparatus (Instron 5566). Wide 5−10 cm strips were uniaxially strained at room temperature and low strain rates (10 mm/min for the composites and 15 mm/min for the polymers) in order to achieve uniform deformation.

Instrumentation. Transmission electron microscopy (TEM, Jeol JEM-2010 with LaB_6 emitter) was performed at an accelerating voltage of 200 kV on samples microtomed by a Leica Ultracut UCT Microtome with cryoattachment. Wide-angle X-ray diffraction (WAXD) was carried out in a Rigaku D/MAX Rapid II instrument equipped with a 2D detector and a graphite monochromator, using a 100 μm pinhole collimator, a 127.4 mm sample-to-detector distance, and Cu K$\alpha_{1,2}$ radiation (λ = 1.5418 Å). The films were measured both with the X-ray beam normal to the film surface (face-on XRD) and with the X-ray beam parallel to the film surface (edge-on XRD). Differential scanning calorimetry (DSC) was carried out in a thermal analysis (TA) Instruments Q100 calorimeter operated at heating and cooling temperature ramps of 10 °C/min under a nitrogen atmosphere. Dielectric breakdown measurements were performed on a TREK P0621P instrument. The specimens were sandwiched between a one-side conducting polypropylene tape (top electrode) and a copper plate (bottom electrode), and all specimens were tested under a dc voltage ramp of 500 V/s.[32] Leakage current was measured under an electric field of 55 MV/m using a Keithley 6517 pA meter with Stanford Research Systems PS 350 as a high-voltage source and was performed at 25 °C in a Sun Electronic EC1A Oven.

RESULTS AND DISCUSSION

Effects of Nanoclay Alignment on the High Field Performance of Polymer Nanocomposites. Composite films with aligned MMT nanofillers are produced in a blown-film line. The blowing process can effectively orient the high-aspect-ratio nanoclays parallel to the film surface, and the flow-induced filler orientation can be increased with increasing shear rate during the manufacturing. Using two-dimensional WAXD in transmission mode through the films, the 2D diffraction patterns of the composite films are collected, as shown in Figure 1a. In the measurements, an X-ray beam is directed either normal to the film surface (face-on) or parallel to the film surface (edge-on). In the face-on configuration, the MMT diffraction patterns are absent, suggesting that the majority of the nanoclay platelets are arranged parallel to the film surface such that most X-ray incident on the nanofillers is reflected back,[33,34] whereas in the edge-on configuration, the diffraction patterns of the MMT nanofillers (high-intensity feature near the beam stop in Figure 1a) become highly azimuthally narrowed. The latter is consistent with large populations of intercalated nanoclays being aligned along the flow direction and can provide a quantitative measure of filler alignment when the relevant diffraction peaks are integrated

DOI: 10.1021/acsanm.8b00671
ACS Appl. Nano Mater. 2018, 1, 3520−3530

azimuthally. Namely, the orientation factor (S_d) for a specific plane can be calculated by Herman's orientation function:[35]

$$S_d = \frac{3\langle\cos^2\phi\rangle - 1}{2} \quad \text{with}$$
$$\langle\cos^2\phi\rangle = \frac{\int_0^{\pi/2} I(\phi)\cos^2\phi \sin\phi \, d\phi}{\int_0^{\pi/2} I(\phi)\sin\phi \, d\phi} \quad (1)$$

$I(\phi)$ are radial intensities; the radial ϕ is defined as $\cos(\phi) = \cos(\beta)\cos(\theta)$ with β being the azimuthal angle and θ being the usual Bragg angle. The orientation factor is calculated for any diffraction peak (hkl) given its background-corrected azimuthal intensities $I(\beta)$ which are then converted to radial intensities $I(\phi)$. $S_d = 0$ denotes a randomly oriented hkl plane and $S_d = -0.5$ a plane oriented along the reference axis (symmetry axis), whereas $S_d = 1$ denotes a plane perpendicular to the reference axis. Figure 1b shows the azimuthally integrated diffraction intensities for MMT basal 001 plane. A high degree of filler orientation is manifested by a strong reflection peak at $\beta = 0$; with increasing shear rate, the peaks become sharper with gradually reduced FWHM, indicating that the filler orientation is enhanced. The orientation factors S_d of the nanoclays are calculated to be 0.70 for the composite film produced at the low shear rate ($1\dot{\gamma}$), increasing to 0.78 at the medium shear rate ($1.42\dot{\gamma}$) and to 0.83 at the high shear rate ($2\dot{\gamma}$), as plotted in Figure 1c. The increased filler orientation with increasing shear rate arises from the higher shear stress in the die and larger elongation flow at the die exist during the blowing process.

The different shear rates can also generate different orientation of polymer crystals, but the subsequent annealing could relax the oriented crystals to some extent. Since crystal orientation has considerable impacts on the high field properties of polymeric dielectrics, it also needs to be evaluated for the blown composite films. As shown in Figure 1a, the diffraction patterns at high angles correspond to PE 110 and PE 200 reflections (the out bright rings). They are much broader than the MMT diffractions, suggesting a lower orientation level for the polymer crystals. The azimuthal intensities of these two diffraction peaks are measured in both face-on and edge-on configurations, and they are nearly identical due to the fiber symmetry of the crystal orientation distribution around the flow direction under the current processing conditions (i.e., the diffraction characteristics would be independent of X-ray beam direction as far as X-ray is normal to the flow direction).[36] As a result, only the face-on profiles are shown in Figure 1b. Based on polymer crystallography, the crystal planes indexed with 00l are the planes of interest, as they are parallel to the lamella surface and normal to the polymer chain direction; however, the diffractions of these planes are absent in the 2D WAXD. Alternatively, the orientation factor of 00l planes can be calculated from the 200 and 110 diffractions, for orthorhombic crystal structures like PE, via[37−39]

$$\langle\cos^2\phi\rangle_{00l} = 1 - 0.555\langle\cos^2\phi\rangle_{200} - 1.445\langle\cos^2\phi\rangle_{110} \quad (2)$$

$\langle\cos^2\phi\rangle_{200}$ and $\langle\cos^2\phi\rangle_{110}$ are the order parameters for PE 200 and PE 110 planes, respectively (eq 1). Figure 1d presents the calculated orientation factors for the 00l planes in the composite films. The polymer crystallites are less aligned than the nanofillers, as the thermal annealing is effective to relax the crystal orientation, but not so much for the oriented nanoclays with a large lateral dimension (up to micrometers). Across different composite films, the orientation factor of the crystals is almost identical (i.e., 0.43 for the film produced at the low shear rate $1\dot{\gamma}$, 0.44 at the medium shear rate $1.42\dot{\gamma}$, and 0.45 at the high shear rate $2\dot{\gamma}$). The slight variation in the crystal orientation cannot account for any appreciable difference in the high field properties of the composites, especially considering the low crystallinity of these composite films (crystallinity for 6 wt % composite is around 35%, Table 1).

Table 1. Crystallinity of the Stretched Polymers and the Stretched Composites

polymer		6 wt % composite		9 wt % composite	
strain (%)	crystallinity (%)	strain (%)	crystallinity (%)	strain (%)	crystallinity (%)
550	36.7	530	39.5	500	39.3
500	38.1	450	39.5	450	39.1
390	37.1	340	37.7	400	39.5
310	35.7	240	38.4	340	38.9
220	37.2	150	37.3	260	37.3
170	36.6	20	35.4	200	38.5
20	34.6	0	36.6	140	35.2
0	32.3			0	35.0

In addition to the crystal and filler alignment, the dispersion of the nanofillers is also critical to the composite performance. Shown in Figure 2a is the cross-section TEM of 6 wt % composite film (high shear rate/high filler orientation). At the micrometer scale, the nanoclay clusters are distributed uniformly across the polymer matrix without any substantial filler aggregation. The nanoclays are highly aligned along the flow direction with the filler surface parallel to the film surface, which is consistent with the previous 2D WAXD measurements (Figure 1a). At the nanometer scale, the organoclays are packed into clusters consisting of a few well-ordered MMT layers down to a single layer. This is the typical morphology for intercalated nanoclays, as can also be reflected from the WXRD measurements. As shown in Figure 2b, all composites exhibit the signature polyolefin/o-MMT intercalated diffraction pattern, with both MMT 001 and MMT 002 peaks present, indicating some level of long-range order (at the multiple-filler length scale) for the organoclays. The interlayer spacing of nanoclays is similar in these composites, ranging from 39.8 Å for the film with high filler orientation to 42.5 Å for the film with low filler orientation. The average cluster size is also similar, as can be manifested by the almost identical FWHM of the MMT 001 diffraction peak in all composites (the actual cluster size cannot be calculated by the data at hand, perhaps due to the existence of disordered nanoclays and/or the instrumental broadening). The nearly identical filler dispersion (intercalated structure, comparable interlayer spacing, and cluster size) in all films can be expected, as it is a direct consequence of the thermodynamically favorable mixing of the nanoclays with the PE matrix, mediated by the inclusion of maleic anhydride functionalized PE and alkylammonium surfactants for the organoclays.[40,41]

The breakdown performances of these composite films are analyzed by a two-parameter Weibull distribution function[42] (eq 3).

DOI: 10.1021/acsanm.8b00671
ACS Appl. Nano Mater. 2018, 1, 3520−3530

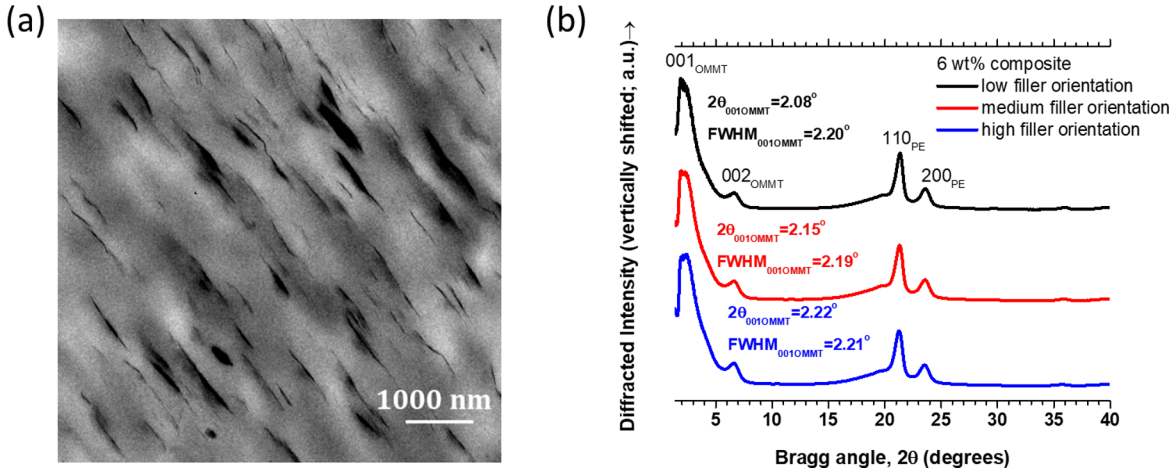

Figure 2. (a) Cross-section TEM images of the blown composite film (high shear rate/high filler orientation). The orientation of the nanofillers along the film surface and along the flow direction can be clearly observed. (b) WAXD patterns of the composite films. The nanoclays in the composite films are intercalated, with similar interlayer spacing and a similar cluster size across all aligned fillers studied (i.e., the average number of layers in the intercalated tactoids is similar).

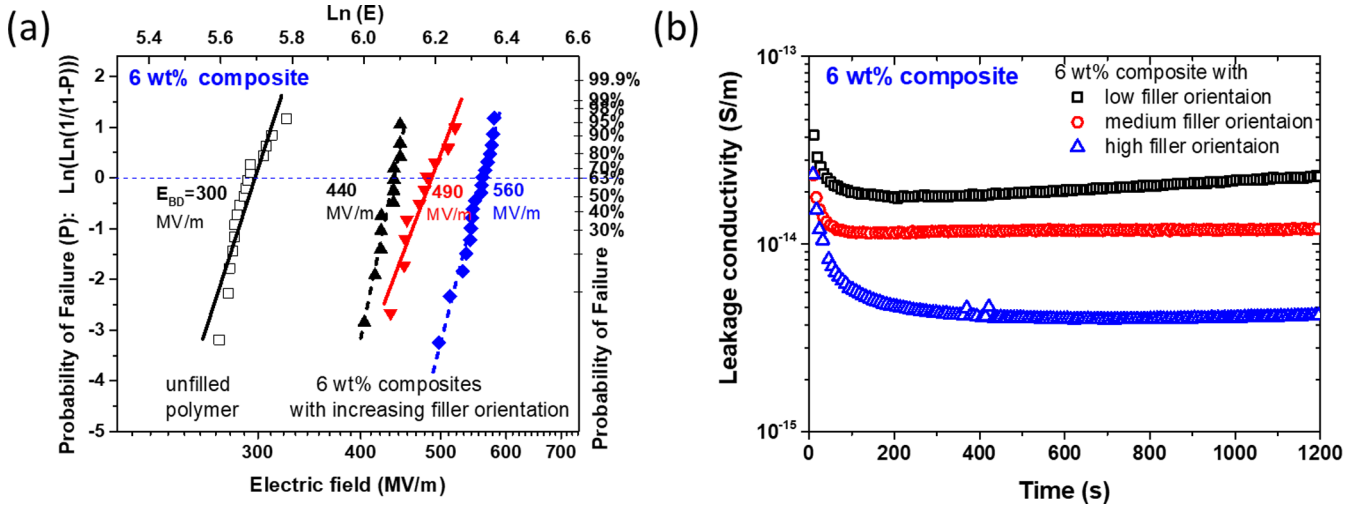

Figure 3. (a) Weibull distribution and characteristic dielectric breakdown strength for the composite films; also included are the results for the unfilled polymer. Addition of aligned fillers can increase the breakdown strength, which is further improved by increasing filler orientation. (b) Electrical conductivity of the composite films under a constant electric field of 55 MV/μm. Increasing filler orientation reduces the leakage current, indicating improved barrier properties with filler alignment.

$$P(E) = 1 - \exp\left(-\left(\frac{E}{E_{BD}}\right)^{\beta_w}\right) \quad (3)$$

$P(E)$ is the cumulative probability of failure occurring at electric fields lower or equal to E. E_{BD} is the field strength under which there is a 63% probability for the sample to fail, also denoted as the characteristic breakdown strength; the shape parameter β_w measures the slope of the fitted Weibull curve, representing the scattering of the experimental data. Figure 3a presents the Weibull plots for the composite films, which clearly shows an increase in breakdown strength with filler orientation. Since the composites produced at different blowing conditions exhibit similar filler dispersion and crystal orientation, the E_{BD} variation can be safely ascribed to the only structural distinction in these composite films—the different nanofiller orientation. With increasing orientation of the nanoclays, more tortuous pathways between and around the aligned nanofillers are necessitated for discharges to propagate.

The assignment of a barrier related mechanism for the E_{BD} improvement can be further confirmed by the following leakage current measurement and the comparison between mechanical and dielectric properties.

Figure 3b shows the electrical conductivities of these composites under a constant electric field. Since the total population of available ions is comparable in all composites (as the three composites have same filler content and similar filler dispersion), the leakage current results can be directly used to evaluate the barrier properties of these composites against mobile charges. As expected, a composite film with a higher filler orientation exhibits a lower leakage conductivity, indicating that the nanoclay orientation indeed improves insulating barrier properties. Figure 4 presents the comparison between the breakdown strengths and the mechanical properties of these composite films. The underlying cause for this comparison is based on the morphological considerations that at a macroscopic level electronic and mechanical performances may not be distinct:[20] i.e., improved mechanical

DOI: 10.1021/acsanm.8b00671
ACS Appl. Nano Mater. 2018, 1, 3520−3530

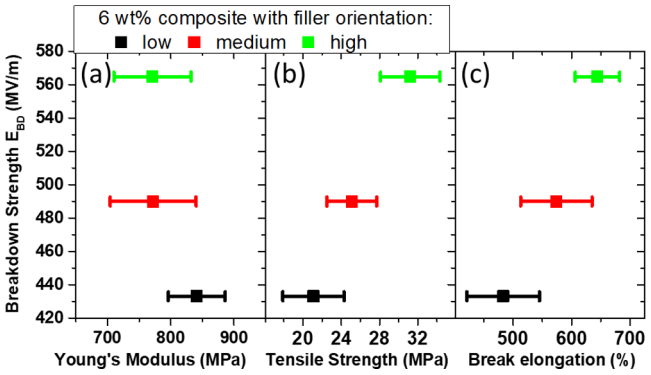

Figure 4. Comparison between the mechanical properties and the dielectric breakdown strength, as a function of increased nanofiller alignment. (a) The decreased E_{BD} with modulus is opposite to the typical behavior of electromechanical failure. (b, c) E_{BD} increases with mechanical strength and toughness, strongly suggesting a barrier related mechanism.

properties—obtained with better filler dispersion and improved polymer/filler interfaces—could lead to enhanced electrical performance. As shown in Figure 4, E_{BD} decreases with mechanical modulus and increases with toughness (break elongation or tensile strength). The former suggests that the E_{BD} improvement is not due to electromechanical reinforcement (otherwise, E_{BD} should be proportional to the square root of mechanical modulus);[43] the latter backs up our postulation of the increased barriers as the dominant reinforcement mechanism—in this case, since E_{BD} measures the resistance to e^- treeing and toughness measures the resistance to crack propagation, they are analogous to each other, both increasing with enhanced barrier properties.

Effects of Crystal Alignment on the High Field Performance of Polymers. Polymers with systematically increased crystal orientation are produced by cold-stretching the unfilled films to different strains. As demonstrated before, the orientation of crystals is evaluated by 2D WAXD. Figure 5a shows the diffraction patterns of the stretched polymer films; Figure 5b records the azimuthal diffraction intensities of the PE 110 and PE 200 planes. Unlike the blowing process where the high-temperature environment could relax polymer crystal orientation, the cold stretching can effectively orient the polymer crystallites, as clearly reflected from the azimuthal narrowing of the crystal diffractions. Following the same approach (eq 2), the orientation factors of the polymer crystals are calculated, with the results are plotted in Figure 5c. A monotonic, albeit nonlinear, increase in the orientation with strain can be identified, corresponding to the structure development from lamellar deformation to fragmentation and eventually toward the formation of fibrillar structures.[44,45]

The crystallinities of the stretched films are also measured, as the strain-induced crystallization could substantially influence the dielectric behaviors of polymers. As summarized in Table 1, for the polymer group, the expected increase in crystallinity with stretching is largely limited, with less than 4% increase over the entire strain range. This result could be related to the fact that all films are heterogeneously nucleated, which already maximizes the crystal fraction, leaving less room for further crystallization to occur. The small increase in the crystallinity cannot be regarded as the dominant factor for any considerable change in the high field properties (Figure S1).

The high field properties of the stretched polymers are investigated in terms of dielectric breakdown and leakage current. The distributions of breakdown fields are analyzed with Weibull statistics (eq 3), as shown in Figure 6a, and the electrical conductivities under a constant electric field are

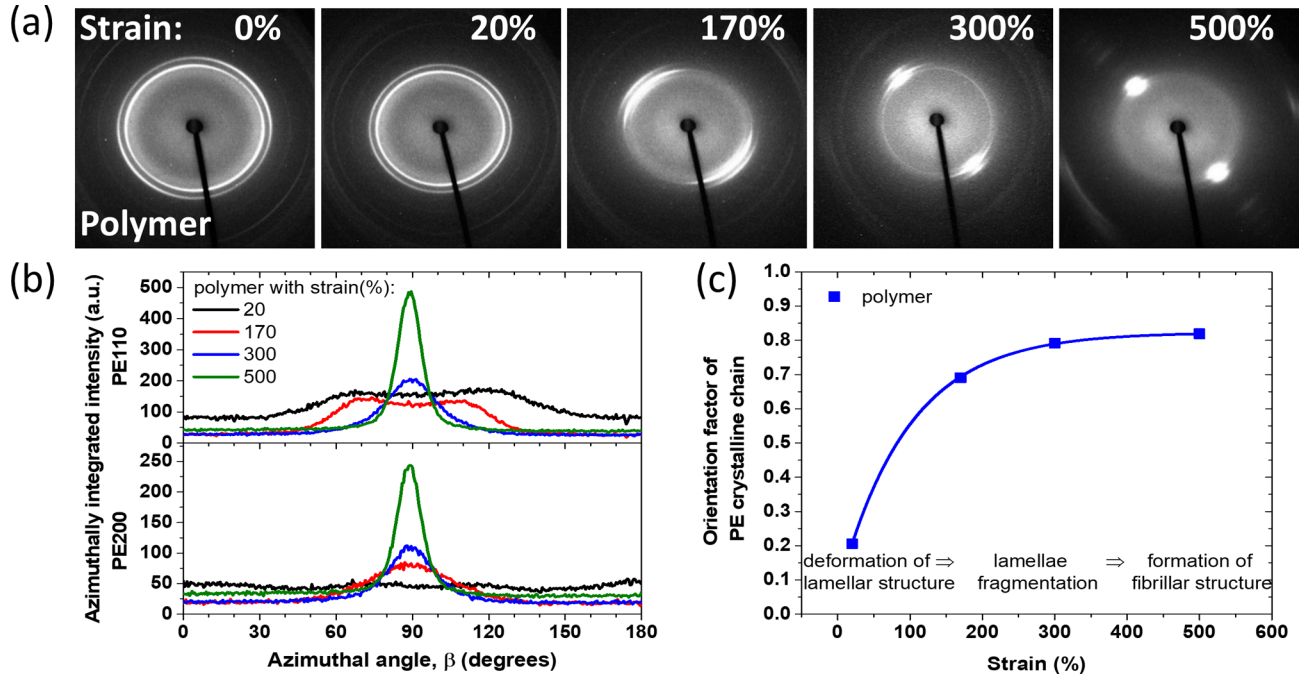

Figure 5. (a) Two-dimensional WAXD patterns for the stretched polymer films at different strains. Crystals are gradually oriented with stretching, as revealed by the azimuthal narrowing of the diffraction patterns of polymer crystal peaks. (b) Azimuthally integrated diffraction intensities from the 2D WAXD patterns shown in (a) for the polymer crystallites. (c) Orientation factor of the crystalline polymer chains as a function of strain in the stretched polymer films.

DOI: 10.1021/acsanm.8b00671
ACS Appl. Nano Mater. 2018, 1, 3520−3530

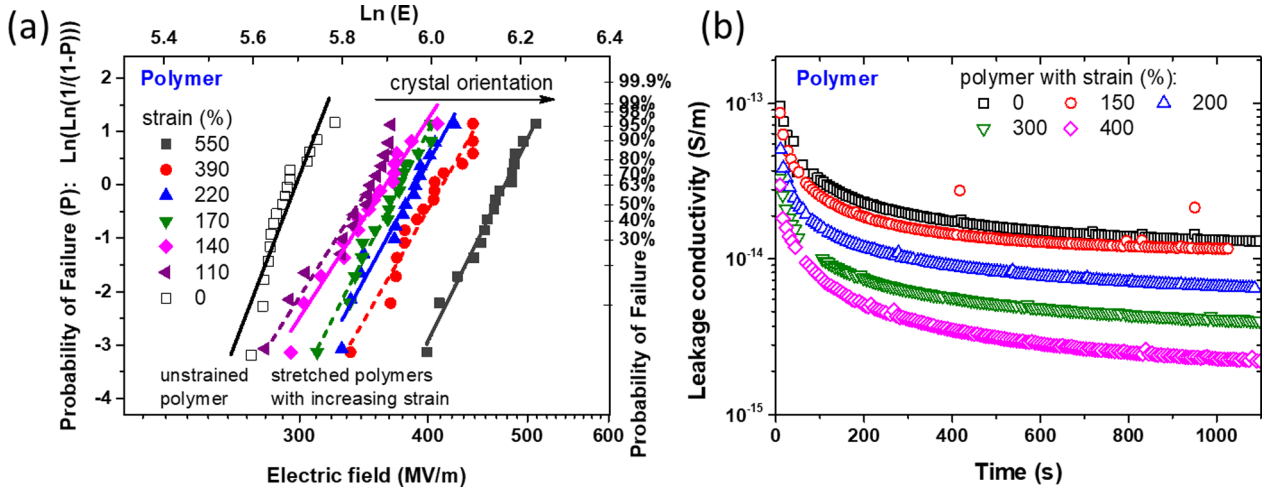

Figure 6. (a) Weibull distribution of breakdown strengths for the stretched unfilled polymer films. The Weibull curve is shifted to the high *E*-field side with stretching/crystal orientation. (b) Electrical conductivity of the stretched polymer films under a constant electric field of 55 MV/μm. Leakage current is reduced with stretching/crystal orientation, indicating improved barrier properties.

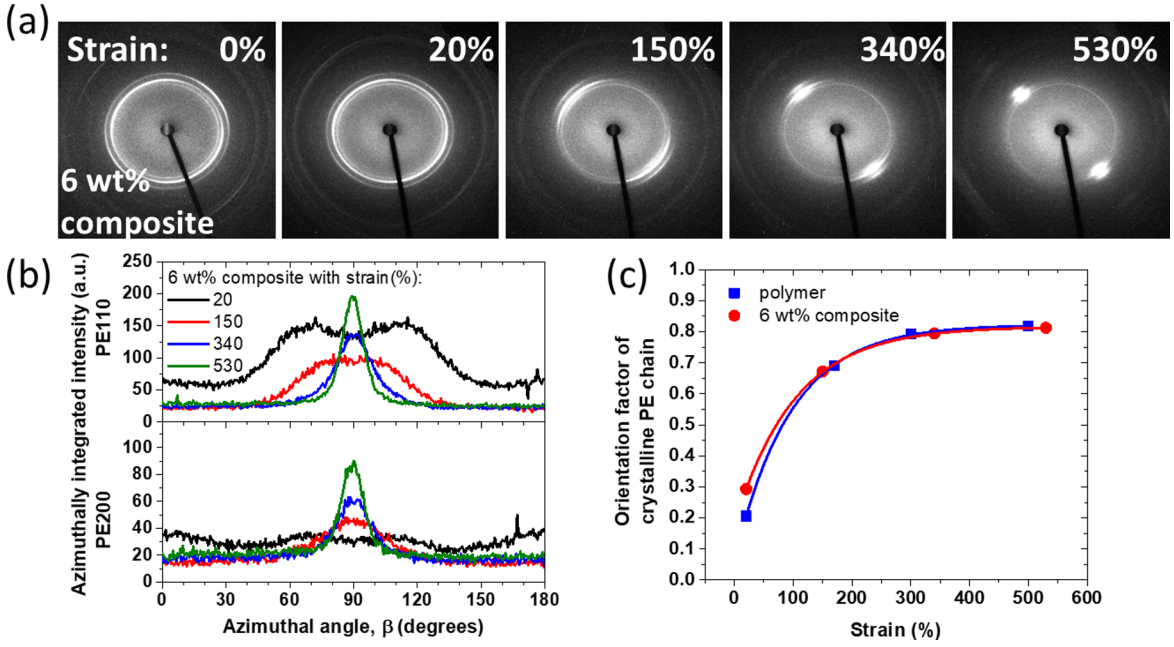

Figure 7. (a) Two-dimensional WAXD patterns for the stretched composite films at different strains. Crystals are gradually oriented with stretching, as revealed by the azimuthal narrowing of the diffraction patterns of the polymer crystal peaks. (b) Azimuthally integrated diffraction intensities from the 2D WAXD patterns shown in (a) for the polymer crystallites. (c) Orientation factor of the crystalline polymer chains as a function of strain for the stretched composite films and for the stretched polymer films. The strain-induced crystal orientation is very similar in the two samples, suggesting that the presence of the nanofillers does not markedly affect the polymer crystal orientation.

presented in Figure 6b. A systematic increase in E_{BD} and decrease in leakage current with strain can be clearly identified, which should be related to the crystal orientation, as it is the main structure change upon stretching. Comparison between Figure 3 and Figure 6 further indicates a similar role of the polymer crystals and the nanoclays in improving the high field properties: increasing orientation of either of them can shift Weibull curves toward the high *E*-field side without changing the distribution of breakdown failures, i.e., β_w is largely unaffected; besides, the E_{BD} enhancement is accompanied by a reduction in the leakage current. These facts strongly imply that the crystal orientation improves the breakdown strength through a similar mechanism as that of the nanofiller orientation—that is, by increasing the path tortuosity for charge transport. This can be understood because compared with amorphous regions, crystals are more ordered in structure, containing fewer impurities and microvoids, and thus can exhibit a stronger resistance for ionization and e^- treeing propagation.[46] With increasing crystal orientation, more obstruction is encountered for discharges, and hence a systematic improvement in the high field properties can be expected.

Since the crystal orientation has an equivalent effect on the high field properties to the nanoclay alignment, one may also wonder whether these two approaches can be synergistically combined to provide an additive improvement in high field dielectric performances. The answer to this question has important practical implications, as it can reduce the necessary

DOI: 10.1021/acsanm.8b00671
ACS Appl. Nano Mater. 2018, 1, 3520−3530

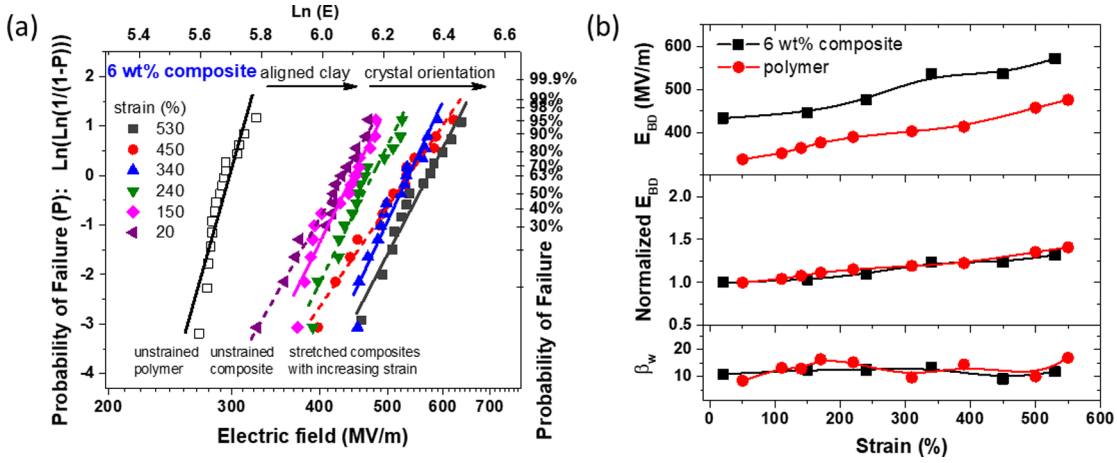

Figure 8. (a) Weibull distribution of breakdown strengths for the stretched composite films (6 wt % organoclays). Addition of the aligned nanofillers shifts the Weibull curve to the high *E*-field side; further stretching/crystal orientation continues to shift the curve toward higher electric fields. The equivalent effect of aligned nanofillers and oriented polymer crystals is indicated. (b) (top) Characteristic breakdown strength of the stretched polymers and the stretched composites. Strain-induced E_{BD} improvement shows the same trend in both samples; introduction of aligned fillers provides an additional systematic increase in E_{BD}. (middle) Normalized E_{BD} curves of the two samples highly overlap with each other, confirming the same extent of E_{BD} increase with strain. (bottom) Weibull modulus is largely unaffected by the stretching or by the addition of the nanofillers, implying a common breakdown mechanism in all samples.

filler concentration in the dielectric polymer composites for the same breakdown performance and can remove the requirement of high crystallinity for the dielectric polymers.

Synergistic Effects of Crystal Orientation and Nanoclay Alignment on the High Field Performance of Polymer Nanocomposites. To answer the above question, the 6 wt % composite film is thermally annealed to further reduce the crystal orientation and then cold stretched to different strains to prepare the composite samples with systematically varied crystal orientation and meanwhile containing the highly aligned nanofillers. The high field properties of these stretched composites are compared with those of the stretched polymers to understand the interaction between the aligned nanoclays and the crystal orientation and their effects on the breakdown performance.

Again, the orientation of polymer crystallites in these stretched composites is evaluated by 2D WAXD, with the diffraction patterns shown in Figure 7a and the azimuthally integrated intensities shown in Figure 7b. The calculated orientation factors of the polymer crystals are depicted in Figure 7c. As expected, the polymer crystal orientation can be increased by cold stretching in the composites. For comparison, also included in Figure 7c are the orientation results of the polymer crystals for the stretched polymers (i.e., Figure 5c). Interestingly, the presence of nanofillers does not affect the crystal orientation, as the orientation factor of crystals is almost the same in the composite and polymer at the same strain. This observation allows us to use the strain as a direct measure of crystal orientation in both films.

The crystallinities of the stretched composites are also measured, as summarized in Table 1. Because of the same reason for heterogeneous nucleation, the strain-induced crystallization is also greatly restricted in the composite films (the crystallinity increase is less than 3% over the strain range); besides, under a certain strain, the composite and polymer show a very similar crystallinity (the difference in crystallinity between the two systems is less than 2% across all specimens at certain strains). The crystallinity variation is too small to exert any appreciable influence on E_{BD} (Figure S1).

As a result, the orientation of crystals is still the major structure change with stretching for the strained composites, and the presence of aligned nanoclays is the main structural distinction between the stretched polymers and the stretched composites.

The distribution of breakdown fields for the stretched composites is analyzed by Weibull function (eq 3), as shown in Figure 8a. The Weibull curves of the stretched composite films resemble closely the curves of the stretched polymer films (Figure 8a vs Figure 3a); i.e., in both films the breakdown fields are improved by stretching, while the slope of Weibull curve remains largely unchanged. This behavior indicates a similar mechanism underlying the strain-induced E_{BD} enhancement for the two series of films. In order to quantify the contribution of crystal orientation and aligned nanofillers, the breakdown strengths of the stretched composites are compared with those of the stretched polymers, as shown in Figure 8b.

At a certain strain, E_{BD} of the composite films is always larger than that of the polymer films by a nearly constant value (ca. 100 MV/m, the top panel of Figure 8b). This E_{BD} difference reflects the contribution from the aligned nanoclays, as it is the main structure difference between the polymers and composites. The aligned nanoclays can act as additional barriers against e^- treeing and hence improve the breakdown strength of the polymer nanocomposites. Moreover, since the nanofillers are already highly aligned in the unstrained composite film (S_d = 0.8), leaving less room for further orientation with stretching, a constant contribution from the nanofillers can be understood. This behavior denotes that an additional number of barriers, which are associated with the aligned fillers and which are nearly independent of strain, are superimposed to any oriented polymer crystal effects. Also, as revealed in the top panel of Figure 8b, E_{BD}−strain curves of the two films are almost parallel to each other, indicating that the same level of E_{BD} increases with strain in both films. It can be more clearly demonstrated by a great overlap between their normalized E_{BD} curves (middle panel of Figure 8b). Since the polymer crystal orientation is still the major structure change upon stretching in the composites and the polymers, and both

DOI: 10.1021/acsanm.8b00671
ACS Appl. Nano Mater. 2018, 1, 3520−3530

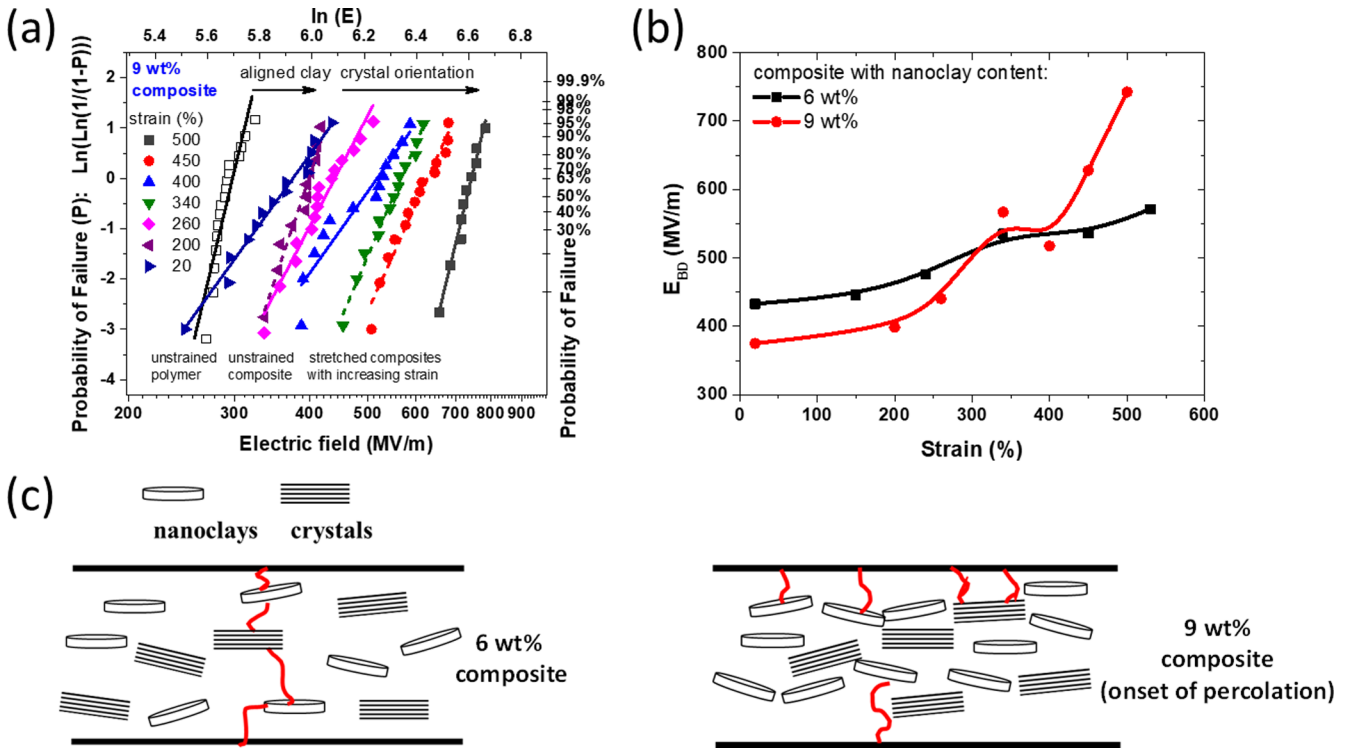

Figure 9. (a) Weibull distribution of breakdown strengths for the stretched composite films (9 wt % organoclays). Addition of the aligned nanofillers shifts the Weibull curve to the high *E*-field side; further stretching/crystal orientation continues to shift the curve toward higher electric fields. (b) Comparison of characteristic breakdown strength between the 6 wt % nanocomposites and the 9 wt % nanocomposites. The high filler loading composites show a bimodal behavior, indicating two different mechanisms operating at low and high strain regions. (c) Schematic depiction of the morphological features in the two nanocomposites. For low filler loading composites, increasing orientation of the nanofillers and the crystals increases the path tortuosity for e^- treeing propagation; for high filler loading composites and at high strains, the aligned nanofillers and oriented crystals can cooperate to establish a macroscopic barrier across the film (partially percolated barrier structure), substantially improving the barrier properties and thus the breakdown performances.

samples show a comparable crystal orientation at a certain strain, this behavior suggests that the same orientation of polymer crystallites improves the barrier properties and thus the breakdown strength, to the same extent in the composite films and polymer films, regardless of with or without fillers. Finally, as depicted in the bottom panel of Figure 8b, the Weibull moduli of the polymers and composites are quite similar, and they are largely unaffected by stretching. It is consistent with our understanding. Since the aligned nanofillers are equivalent to the aligned crystals, both acting as barriers to improve the breakdown performance, all studied samples—regardless of with or without nanofillers or under different stretching ratios—are qualitatively the same; i.e., they differ only in the number and distribution of barriers while everything else remains the same. It also implies that the dominant breakdown mechanism does not change in the two series of films.

From the above discussion, it is known that the aligned nanoclays are not unlike the crystal orientation in improving the breakdown performance; they are also independent, since the presence of the nanofillers does not affect the crystal orientation or influence its contribution to E_{BD}, and vice versa; moreover, the incorporation of the aligned nanoclays can provide an additional increase in E_{BD}, adding to any improvement that can be obtained by crystal orientation, implying that the two effects are also additive. As a result, a question naturally arises whether we can further strengthen the barrier effects toward the establishment of a percolated barrier structure by combining both effects; apparently, the breakdown strength in this structure can be significantly enhanced. It is still worth mentioning that any attempts to build such percolated morphology in traditional materials will be very challenging if only one mechanism is utilized because it necessitates extremely high filler loadings or large polymer crystallinities. By integrating the two mechanisms (i.e., aligned nanoclays and oriented crystals), it is possible to achieve the percolation of barriers at a reasonable filler concentration and crystallinity. In the studied system, since the polymer crystallinity is stabilized by heterogeneous nucleation, and the nanoclays and crystals already reach a high level of orientation at large strains, the simple way to further improve the barrier properties is to include more aligned nanoclays.

Figure 9a presents the Weibull distribution of breakdown strengths for the stretched composite films with higher filler loading (9 wt % aligned nanoclays). The characteristic E_{BD} of the stretched 9 wt % composites is plotted as a function of strain, as shown in Figure 9b; also included are the breakdown results of the stretched 6 wt % composites. At low strains, E_{BD}–strain curves of the two composites are almost parallel to each other, indicating the same operating mechanism that the strain-induced E_{BD} improvement mainly comes from crystal orientation; at large strains, the curve of the 9 wt % composite begins to deviate from the curve of the 6 wt % composite, showing a stronger upturn. The substantially large and strain-dependent increase in E_{BD} is consistent with our expectation, which should arise from the onset of percolation. At a high

DOI: 10.1021/acsanm.8b00671
ACS Appl. Nano Mater. 2018, 1, 3520−3530

filler loading, the gradually oriented crystals can cooperate with the aligned nanofillers to promote the formation of a macroscopic barrier across the film. This percolated barrier structure can lead to a pronounced increase in E_{BD} by effectively scattering the mobile charges and disrupting the treeing progress (Figure 9c). Finally, at a strain of 500%, the breakdown strength of the stretched composite reaches 750 MV/m, almost 2.5 times E_{BD} of the pristine polymer (unfilled and unstrained polymer). To our best knowledge, the recorded E_{BD} value is also among the largest value ever reported for LLDPE polymer composites.

CONCLUSIONS

In this work, we explore an approach to obtain a high-performance polymer nanocomposite with substantially improved breakdown strength and concurrently reduced leakage current via morphology tailoring—through the controlled alignment of MMT nanoclays and polymer crystals. The effects of nanofiller orientation and crystal orientation and their synergy on the high field properties of structured polymer nanocomposites are systematically studied. It is shown that the aligned MMT nanoclays are equivalent to the oriented crystals in improving the dielectric performances, both acting as extra barriers for charge transport and e^- treeing propagation. Moreover, the contribution from the aligned 2D nanofillers can be synergistically added to that of the crystal orientation in the nanocomposites. At low filler concentration, introduction of the aligned nanofillers provides an additional nontrivial increase in E_{BD}, superimposed on any E_{BD} improvement that can be obtained from the polymer crystal orientation (aligned nanofillers serve as independent barriers). At high filler concentration, a significant improvement in E_{BD} can be achieved at high strains, most probably due to the formation of a macroscopic barrier across the film (aligned nanofillers cooperate with oriented crystals to promote percolation of barriers). The breakdown strength of the strained high-filler-loading composites can reach up to 750 MV/m, among the largest ever reported for LLDPE composites, with unfilled LLDPE having just 300 MV/m. Given that the "structured" polymer nanocomposites can achieve a concurrent increase of E_{BD} and decrease of loss, opposite to the property trade-off of conventional composites (where increases in E_{BD} are usually accompanied by increases in losses), this aligned nanostructure approach can have a profound impact on the development of future high-performance polymeric materials for insulation and for energy storage.

ASSOCIATED CONTENT

Supporting Information

The Supporting Information is available free of charge on the ACS Publications website at DOI: 10.1021/acsanm.8b00671.

Figure S1 (PDF)

AUTHOR INFORMATION

Corresponding Authors

*E-mail: bolipsu@gmail.com (B.L.).
*E-mail: manias@psu.edu (E.M.).

ORCID

Bo Li: 0000-0002-4890-8435

Notes

The authors declare no competing financial interest.

ACKNOWLEDGMENTS

This work was supported by the National Science Foundation, as part of the Center for Dielectrics and Piezoelectrics under Grants IIP-1361571 and IIP-1361503. Additional support through CSC and ΓΓΕΤ fellowships is acknowledged by B.L. and P.I.X., respectively. The authors are grateful to PolyK Technologies for the electrical measurements.

REFERENCES

(1) Liu, F.; Li, Q.; Cui, J.; Li, Z.; Yang, G.; Liu, Y.; Dong, L.; Xiong, C.; Wang, H.; Wang, Q. High-Energy-Density Dielectric Polymer Nanocomposites with Trilayered Architecture. *Adv. Funct. Mater.* **2017**, *27*, 1606292.

(2) Azizi, A.; Gadinski, M. R.; Li, Q.; AlSaud, M. A.; Wang, J.; Wang, Y.; Wang, B.; Liu, F.; Chen, L. Q.; Alem, N.; Wang, Q. High-Performance Polymers Sandwiched with Chemical Vapor Deposited Hexagonal Boron Nitrides as Scalable High-Temperature Dielectric Materials. *Adv. Mater.* **2017**, *29*, 1701864.

(3) Wang, Y. F.; Wang, L. X.; Yuan, Q. B.; Niu, Y. J.; Chen, J.; Wang, Q.; Wang, H. Ultrahigh Electric Displacement and Energy Density in Gradient Layer-Structured $BaTiO_3$/PVDF Nanocomposites with An Interfacial Barrier Effect. *J. Mater. Chem. A* **2017**, *5*, 10849−10855.

(4) Li, Q.; Liu, F.; Yang, T.; Gadinski, M. R.; Zhang, G.; Chen, L. Q.; Wang, Q. Sandwich-structured Polymer Nanocomposites with High Energy Density and Great Charge-Discharge Efficiency at Elevated Temperatures. *Proc. Natl. Acad. Sci. U. S. A.* **2016**, *113*, 9995−10000.

(5) Hanley, T. L.; Burford, R. P.; Fleming, R. J.; Barber, K. W. A General Review of Polymeric Insulation for Use in HVDC Cables. *IEEE Electr. Insul. Mag.* **2003**, *19*, 13−24.

(6) Khanchaitit, P.; Han, K.; Gadinski, M. R.; Li, Q.; Wang, Q. Ferroelectric Polymer Networks with High Energy Density and Improved Discharged Efficiency for Dielectric Energy Storage. *Nat. Commun.* **2013**, *4*, 2845.

(7) Vaia, R. A.; Maguire, J. F. Polymer Nanocomposites with Prescribed Morphology: Going beyond Nanoparticle-Filled Polymers. *Chem. Mater.* **2007**, *19*, 2736−2751.

(8) Roy, M.; Nelson, J.; MacCrone, R.; Schadler, L.; Reed, C.; Keefe, R.; Zenger, W. Polymer Nanocomposite Dielectrics-The Role of The Interface. *IEEE Trans. Dielectr. Electr. Insul.* **2005**, *12*, 629−643.

(9) Grabowski, C. A.; Fillery, S. P.; Westing, N. M.; Chi, C.; Meth, J. S.; Durstock, M. F.; Vaia, R. A. Dielectric Breakdown in Silica−Amorphous Polymer Nanocomposite Films: The Role of the Polymer Matrix. *ACS Appl. Mater. Interfaces* **2013**, *5*, 5486−5492.

(10) Roy, M.; Nelson, J. K.; MacCrone, R. K.; Schadler, L. S. Candidate Mechanisms Controlling The Electrical Characteristics of Silica/XLPE Nanodielectrics. *J. Mater. Sci.* **2007**, *42*, 3789−3799.

(11) Li, Q.; Zhang, G.; Liu, F.; Han, K.; Gadinski, M. R.; Xiong, C.; Wang, Q. Solution-processed Ferroelectric Terpolymer Nanocomposites with High Breakdown Strength and Energy Density Utilizing Boron Nitride Nanosheets. *Energy Environ. Sci.* **2015**, *8*, 922−931.

(12) Xie, Y.; Wang, J.; Yu, Y.; Jiang, W.; Zhang, Z. Enhancing Breakdown Strength and Energy Storage Performance of PVDF-based Nanocomposites by Adding Exfoliated Boron Nitride. *Appl. Surf. Sci.* **2018**, *440*, 1150−1158.

(13) Tomer, V.; Manias, E.; Randall, C. A. High Field Properties and Energy Storage in Nanocomposite Dielectrics of Poly(vinylidene fluoride-hexafluoropropylene). *J. Appl. Phys.* **2011**, *110*, 044107.

(14) Fillery, S. P.; Koerner, H.; Drummy, L.; Dunkerley, E.; Durstock, M. F.; Schmidt, D. F.; Vaia, R. A. Nanolaminates: Increasing Dielectric Breakdown Strength of Composites. *ACS Appl. Mater. Interfaces* **2012**, *4*, 1388−1396.

(15) Lewis, T. J. Interfaces: Nanometric Dielectrics. *J. Phys. D: Appl. Phys.* **2005**, *38*, 202−212.

(16) Lewis, T. J. Nanometric Dielectrics. *IEEE Trans. Dielectr. Electr. Insul.* **1994**, *1*, 812−825.

(17) Borgani, R.; Pallon, L. K. H.; Hedenqvist, M. S.; Gedde, U. W.; Haviland, D. B. Local Charge Injection and Extraction on Surface-

DOI: 10.1021/acsanm.8b00671
ACS Appl. Nano Mater. 2018, 1, 3520−3530

Modified Al_2O_3 Nanoparticles in LDPE. *Nano Lett.* **2016**, *16*, 5934−5937.
(18) Tanaka, T.; Kozako, M.; Fuse, N.; Ohki, Y. Proposal of A Multi-Core Model for Polymer Nanocomposite Dielectrics. *IEEE Trans. Dielectr. Electr. Insul.* **2005**, *12*, 669−681.
(19) Smith, R. C.; Liang, C.; Landry, M.; Nelson, J. K.; Schadler, L. S. The Mechanisms Leading To The Useful Electrical Properties of Polymer Nanodielectrics. *IEEE Trans. Dielectr. Electr. Insul.* **2008**, *15*, 187−196.
(20) Tomer, V.; Polizos, G.; Randall, C. A.; Manias, E. Polyethylene Nanocomposite Dielectrics: Implications of Nanofiller Orientation on High Field Properties and Energy Storage. *J. Appl. Phys.* **2011**, *109*, 074113.
(21) Li, B.; Manias, E. Increased Dielectric Breakdown Strength of Polyolefin Nanocomposites via Nanofiller Alignment. *MRS Adv.* **2017**, *2*, 357−362.
(22) Hosier, I. L.; Vaughan, A. S.; Swingler, S. G. On The Effects of Morphology and Molecular Composition on The Electrical Strength of Polyethylene Blends. *J. Polym. Sci., Part B: Polym. Phys.* **2000**, *38*, 2309−2322.
(23) Hosier, I. L.; Vaughan, A. S.; Swingler, S. G. Structure−Property Relationships in Polyethylene Blends: The Effect of Morphology on Electrical Breakdown Strength. *J. Mater. Sci.* **1997**, *32*, 4523−4531.
(24) Lewis, T. J. Polyethylene Under Electrical Stress. *IEEE Trans. Dielectr. Electr. Insul.* **2002**, *9*, 717−729.
(25) Jones, J. P.; Llewellyn, J. P.; Lewis, T. J. The Contribution of Field-Induced Morphological Change to The Electrical Aging and Breakdown of Polyethylene. *IEEE Trans. Dielectr. Electr. Insul.* **2005**, *12*, 951−966.
(26) Gao, L. Y.; Tu, D. M.; Zhou, S. C.; Zhang, Z. L. The Influence of Morphology on the Electrical Breakdown Strength of Polypropylene Film. *IEEE Trans. Electr. Insul.* **1990**, *25*, 535−540.
(27) Hozumi, N.; Ishida, M.; Okamoto, T.; Fukagawa, H. The Influence of Morphology on Electrical Tree Initiation in Polyethylene under AC and Impulse Voltages. *IEEE Trans. Electr. Insul.* **1990**, *25*, 707−714.
(28) Tanaka, T.; Okamoto, T.; Hozumi, N.; Suzuki, K. Interfacial Improvement of XLPE Cable Insulation at Reduced Thickness. *IEEE Trans. Dielectr. Electr. Insul.* **1996**, *3*, 345−350.
(29) Li, B.; Xidas, P. I.; Triantafyllidis, K. S.; Manias, E. Effect of Crystal Orientation and Nanofiller Alignment on Dielectric Breakdown of Polyethylene/Montmorillonite Nanocomposites. *Appl. Phys. Lett.* **2017**, *111*, 082906.
(30) Li, B.; Camilli, C. I.; Xidas, P. I.; Triantafyllidis, K. S.; Manias, E. Structured Polyethylene Nanocomposites: Effects of Crystal Orientation and Nanofiller Alignment on High Field Dielectric Properties. *MRS Adv.* **2017**, *2*, 363−368.
(31) Hozumi, N.; Okamoto, T.; Fukagawa, H. TEM Observation of Electrical Tree Paths and Microstructures in Polyethylene. *Jpn. J. Appl. Phys.* **1988**, *27*, 1230−1233.
(32) Tomer, V.; Randall, C. A. High Field Dielectric Properties of Anisotropic Polymer-Ceramic Composites. *J. Appl. Phys.* **2008**, *104*, 074106.
(33) Fereydoon, M.; Tabatabaei, S. H.; Ajji, A. X-ray and Trichroic Infrared Orientation Analyses of Uniaxially Stretched PA6 and MXD6 Nanoclay Composite Films. *Macromolecules* **2014**, *47*, 2384−2395.
(34) Galgali, G.; Agarwal, S.; Lele, A. Effect of Clay Orientation on The Tensile Modulus of Polypropylene−Nanoclay Composites. *Polymer* **2004**, *45*, 6059−6069.
(35) Koerner, H.; Luo, Y.; Li, X.; Cohen, C.; Hedden, R. C.; Ober, C. K. Structural Studies of Extension-Induced Mesophase Formation in Poly(diethylsiloxane) Elastomers: In Situ Synchrotron WAXS and SAXS. *Macromolecules* **2003**, *36*, 1975−1981.
(36) Schrauwen, B. A. G.; Breemen, L. C. A. v.; Spoelstra, A. B.; Govaert, L. E.; Peters, G. W. M.; Meijer, H. E. H. Structure, Deformation, and Failure of Flow-Oriented Semicrystalline Polymers. *Macromolecules* **2004**, *37*, 8618−8633.
(37) Wilchinsky, Z. W. Determination of Orientation of The Crystalline And Amorphous Phases In Polyethylene by X-ray Diffraction. *J. Polym. Sci. B Polym. Phys.* **1968**, *6*, 281−288.
(38) Che, J.; Locker, C. R.; Lee, S.; Rutledge, G. C.; Hsiao, B. S.; Tsou, A. H. Plastic Deformation of Semicrystalline Polyethylene by X-ray Scattering: Comparison with Atomistic Simulations. *Macromolecules* **2013**, *46*, 5279−5289.
(39) Cai, J.; Hsiao, B. S.; Gross, R. A. Real-Time Structure Changes during Uniaxial Stretching of Poly (omega-pentadecalactone) by in Situ Synchrotron WAXD/SAXS Techniques. *Macromolecules* **2011**, *44*, 3874−3883.
(40) Manias, E.; Touny, A.; Wu, L.; Strawhecker, K.; Lu, B.; Chung, T. C. Polypropylene/Montmorillonite Nanocomposites. Review of the Synthetic Routes and Materials Properties. *Chem. Mater.* **2001**, *13*, 3516−3523.
(41) Vaia, R. A.; Giannelis, E. P. Lattice Model of Polymer Melt Intercalation in Organically-Modified Layered Silicates. *Macromolecules* **1997**, *30*, 7990−7999.
(42) Weibull, W. A Statistical Distribtuion Function of Wide Applicability. *J. Appl. Mech.* **1951**, *18*, 293−297.
(43) Fothergill, J. C. *Electrical Degradation and Breakdown in Polymers*; IET: London, 1992.
(44) Bowden, P. B.; Young, R. J. Deformation Mechanisms in Crystalline Polymers. *J. Mater. Sci.* **1974**, *9*, 2034−2051.
(45) Men, Y.; Rieger, J.; Lindner, P.; Enderle, H.-F.; Lilge, D.; Kristen, M. O.; Mihan, S.; Jiang, S. Structural Changes and Chain Radius of Gyration in Cold-Drawn Polyethylene after Annealing: Small- and Wide-Angle X-ray Scattering and Small-Angle Neutron Scattering Studies. *J. Phys. Chem. B* **2005**, *109*, 16650−16657.
(46) Ieda, M. Electrical Conduction and Carrier Traps In Polymeric Materials. *IEEE Trans. Electr. Insul.* **1984**, *EI-19*, 162−178.

DOI: 10.1021/acsanm.8b00671
ACS Appl. Nano Mater. 2018, 1, 3520−3530